JASA ARTICLE

A broadband active sound absorber with adjustable absorption coefficient and bandwidth

Kangkang Wang,[1] Li Shi,[1] Haishan Zou,[1,a)] Sipei Zhao,[2] Chen Shen,[3] and Jing Lu[1]
[1]*Key Laboratory of Modern Acoustics, MOE, Institute of Acoustics, Department of Physics, Nanjing University, Nanjing 210093, People's Republic of China*
[2]*Centre for Audio, Acoustics and Vibration, Faculty of Engineering and IT, University of Technology Sydney, Ultimo NSW 2007, Australia*
[3]*Department of Mechanical Engineering, Rowan University, Glassboro, New Jersey 08028, USA*

ABSTRACT:
Broadband adjustable sound absorbers are desired for controlling the acoustic conditions within enclosed spaces. Existing studies on acoustic absorbers, either passive or active, aim to maximize the sound absorption coefficients over an extended frequency band. By contrast, this paper introduces a tunable acoustic absorber, whose working frequency band and sound absorption characteristics can be defined by users for different applications. The approach leverages an error signal that can be synthesized using a standing wave separation technique. The error signal encodes different target reflection coefficients, leading to arbitrary absorption coefficients between 0 and 1. Experimental validation is conducted in a one-dimensional standing wave tube, demonstrating that the proposed active absorber achieves near-perfect absorption within the 150–1600 Hz frequency range, boasting an average absorption coefficient of 0.98. Adjustable absorption is demonstrated across three octave bands, aligning closely with theoretical predictions. Furthermore, when coupled with a shaping filter, the absorber exhibits spectrally tunable broadband absorption capabilities, selectively reflecting specific frequency bands while effectively absorbing others. These outcomes underscore the versatile tunability of the proposed active acoustic absorber, which is expected to pave the way for personalized regulating of the indoor acoustic environment.
https://doi.org/10.1121/10.0028196
(Received 26 April 2024; revised 12 July 2024; accepted 25 July 2024; published online 13 August 2024)
[Editor: Yong Li] Pages: 1048–1057

I. INTRODUCTION

As urbanization progresses, multipurpose rooms integrating audio rooms, concert halls, and theatres are increasingly favored for their cost-effectiveness.[1] Different functions in a multipurpose room require different acoustic characteristics, with audio rooms requiring a low reverberation time to increase speech intelligibility, while concert halls and theatres require a certain amount of reverberation for optimal auditory experience. Traditionally, room reverberation has been manipulated through methods like rotatable walls or rollable curtains to alter the absorption area of the room walls.[2] However, these approaches are often unwieldy and demand considerable space, particularly for managing low-frequency sound waves. Therefore, the development of flexibly adjustable broadband absorbers is imperative to regulate room acoustics and achieve cost-effective multifunctional spaces. Although diffusion is also a significant factor in room acoustics and can be adjusted using diffusers, this paper primarily focuses on sound absorption.

In recent years, the emergence of metamaterials has expanded the design possibilities for tunable absorbers. Various subwavelength absorbers based on Helmholtz resonators,[3–12] spatially folded Fabry–Perot (FP) resonators,[13–20] and thin-film structures,[21–26] have been proposed. These absorbers offer adjustable acoustic absorption characteristics achieved by modifying parameters, such as the neck opening size[5–10] and cavity volume[11,12] of the Helmholtz resonators, the effective length of the FP resonators,[15–19] and the additional mass block of the thin-film structures.[21,22] These absorbers have shown promise in controlling sound fields in room acoustics. For example, Qu *et al.*[27] designed a metamaterial absorber using a hybrid structure comprising Helmholtz resonators and FP resonators to manipulate the reverberation characteristics of a small room. This absorber can be precisely adjusted to achieve a reverberation time of 0.1 s. A meta-equalizer is also proposed based on a combined resonator structure. By manually switching on/off the resonators, functional filters, signal reproductions, and sound-effect controls can be implemented.[28] Additionally, utilizing the thermoacoustic effect is also a potential technical solution to design tunable sound absorbers.[29,30] However, their passive nature inherently restricts their tunability. Adjusting their acoustic performance often necessitates mechanically altering their physical structures, posing practical challenges in real-world applications.

To enhance the flexibility of regulating resonator characteristics, active control methods can be introduced. Helmholtz resonators based on program-controlled motors

a)Email: hszou@nju.edu.cn

https://doi.org/10.1121/10.0028196

have been proposed,[31] whose resonance frequency can be flexibly adjusted. A metasurface designed using 200 such tunable resonators can efficiently modulate the reverberant sound field in a room for cross talk–free acoustic communication. An active resonator can also be designed based on impedance synthesis,[32] which enables effective control of the resonant frequency and bandwidth. Additionally, some scholars suggested that the voltage[24] or magnetic field[26] can be applied to control the internal tension of the thin-film structures to modulate the sound absorption performance of thin-film absorbers. Although these structures provide certain adjustability, their strong resonance characteristics make them effective only in a narrow bandwidth around the resonance frequency, which limits their broader applicability.

Recently, the shunt loudspeaker has garnered significant attention as a promising option for designing tunable absorbers with broader bandwidth. This approach is based on the idea of impedance synthesis, which can adjust the acoustic impedance of the loudspeaker diaphragm by modulating the electrical impedance of the shunt circuit. Cong *et al.*[33] devised a multi-resonance shunt circuit to expand the absorption bandwidth of the shunt loudspeaker. Subsequently, they assessed the sound absorption capabilities of an array comprising 64 dual-resonance shunted loudspeakers in a diffuse sound field within a reverberant room, achieving near-perfect absorption at 100 and 200 Hz.[34] Zhang *et al.*[35,36] introduced the concept of a shunted electro-magnetic diaphragm (SEMD), which is characterised by a resistance-inductance-capacitance shunt circuit based on a negative impedance converter to counteract the mechanical impedance of the loudspeaker, thereby enabling broadband sound absorption. Zhang *et al.*[36] presented an extensive parametric analysis of shunted loudspeakers and proposed a methodology for designing broadband tunable sound absorbers. Additionally, the shunt loudspeaker can be combined with other acoustic materials to enhance its performance, such as broadening the absorption band when combined with a microperforated plate.[35,37–39] Nevertheless, as a semi-active absorber, the tunability of the shunt loudspeaker remains constrained, necessitating alterations to the resistance, inductance, or capacitance in the shunt circuit to modulate its sound absorption performance.

Active impedance synthesis with sensors can further enhance the sound absorption capacity and modulation potential of a shunt loudspeaker, which can be programmed with a digital controller to achieve a targeted impedance without changing any components within the circuit. Boulandet and Lissek[40] conducted a comparative study on the efficacy of proportional feedback control, proportional-integral-derivative (PID) control, and phase-compensated control methods. Their findings indicate that PID and phase-compensated control techniques yield superior results by mitigating the adverse effects of higher-order vibration modes in the loudspeaker diaphragm. Rivet *et al.*[41] proposed the control of current rather than voltage to drive the loudspeaker, aiming to circumvent the deterioration of high-frequency acoustic absorption by voice coil inductance and effectively broaden the absorption bandwidth. Furthermore, a novel device, called plasmacoustic metalayers, is proposed to achieve impedance synthesis through feedback control, enabling near-perfect acoustic absorption in the 20–2000 Hz frequency band.[42] However, precise identification of the loudspeaker's Thiele–Small (TS) parameters is crucial for this non-adaptive control approach, and inevitable identification deviation will deteriorate the sound absorption effect. Although mixed feedforward–feedback architecture can help alleviate this problem,[43] the modelling process for loudspeaker-based active impedance synthesis techniques primarily accounts for the piston vibration mode, neglecting higher-order vibration modes, thus inherently constraining their effective bandwidth.

Adaptive active control techniques offer alternatives for absorber design, circumventing the need for precise identification of loudspeakers' TS parameters. Beyene and Burdisso[44] proposed an active–passive hybrid absorber employing an impedance matching strategy to actively cancel the reflected waves separated by the two-microphone method, achieving efficient absorption over a broad bandwidth (100–2000 Hz) with a coefficient exceeding 0.8. Additionally, Cobo *et al.*[45] developed an analytical model to compare the efficacy of impedance matching and pressure release strategies. It is revealed that the pressure release method outperforms impedance matching when the flow resistance of porous materials matches air's characteristic acoustic impedance. Subsequently, a large-area active absorber panel was designed based on the pressure release strategy, and it could achieve up to 0.94 absorption in the frequency range of 266–1500 Hz, even for obliquely incident waves at a 20° angle of incidence.[46] Because of these hybrid active absorbers, combining active units with passive absorbing materials in a cascade form often results in considerable thickness. Employing adaptive impedance control techniques, An *et al.*[47] proposed a hybrid absorber with a parallel form with a thickness of only 80 mm and an absorption performance exceeding 0.9 above 20 Hz. However, most of these studies focus on enhancing sound absorption efficiency across a broader frequency range, and the broadband tunability of active absorbers remains largely unexplored.

In this paper, we present a flexibly tunable active sound absorber, which can attain arbitrary absorption coefficients ranging from 0 to 1 across more than three octave bands by regulating the target reflection coefficient. Moreover, in combination with the filtered-e least mean square (FeLMS) algorithm[48] and a band-stop filter, this active absorber can achieve spectrally tunable broadband acoustic absorption. Experiments are conducted to exemplify the flexible tunability of the designed active absorber, without necessitating any alterations to its physical structure. This absorber is expected to provide a rich means of adjustment for the individualized acoustic environment requirements of multipurpose rooms.

The remainder of this paper is organized as follows. Section II presents the control mechanism and algorithm of our active absorber, which are compared with the existing

design scheme. In Sec. III, experiments are carried out in a standing wave tube to validate the effectiveness of the designed active absorber, and arbitrarily adjustable absorption coefficients between 0 and 1 are realized. Subsequently, a spectrally tunable broadband absorption effect is demonstrated with the use of a band-stop filter. Finally, conclusions are summarized in Sec. IV.

II. THEORY

The configuration of the active sound absorber is shown in Fig. 1. The physical structure of the absorber is marked in the red dashed box, and consists of a loudspeaker in air and the cavity between the loudspeaker and the hard boundary backing. Two microphones, M1 and M2, are located in front of the absorber and are utilized to separate the incident and reflected waves in the one-dimensional standing wave tube to generate the error signal, which is related to the incident wave, the reflected wave, and the target reflection coefficient. The energy of the error signal is minimized by manipulating the secondary source through a controller, facilitating broadband control with adjustable acoustic absorption performance.

A. Current active absorber

Let the incident wave sound pressure be $p_i(t)$ and the reflected wave sound pressure be $p_r(t)$ at microphone M1, then the total sound pressure $p_1(t)$ is

$$p_1(t) = p_i(t) + p_r(t). \tag{1}$$

When the spacing between microphones M1 and M2 is s, the acoustic time delay between them is $\tau = s/c_0$, where c_0 is the speed of sound in air. Moreover, given that the tube's radius is significantly larger than the boundary layer thickness and this paper focuses on low and medium frequency bands below 2000 Hz, the viscothermal loss of sound waves in this tube is minimal and can be reasonably neglected. Therefore, the total sound pressure $p_2(t)$ at microphone M2 can be expressed as

$$p_2(t) = p_i(t-\tau) + p_r(t+\tau). \tag{2}$$

The Fourier transform of Eqs. (1) and (2) yields

$$P_1(\omega) = P_i(\omega) + P_r(\omega), \tag{3}$$

$$P_2(\omega) = P_i(\omega)e^{-j\omega\tau} + P_r(\omega)e^{j\omega\tau}. \tag{4}$$

The incident and reflected waves can be extracted from Eqs. (3) and (4) as follows:

$$P_i(\omega)(e^{-2j\omega\tau} - 1) = P_2(\omega)e^{-j\omega\tau} - P_1(\omega), \tag{5}$$

$$P_r(\omega)e^{j\omega\tau}(e^{-2j\omega\tau} - 1) = P_1(\omega)e^{-j\omega\tau} - P_2(\omega). \tag{6}$$

The primary objective of current active absorber designs is to achieve efficient broadband sound absorption by cancelling reflected waves.[44,49] Control algorithms for such systems often leverage the filtered-x least mean square (FxLMS) algorithm,[50] whose module diagram is depicted in Fig. 2. In this diagram, $W(z)$ represents the z-transform[51] of the control filter $\mathbf{w}(n)$. $x(n)$ refers to the reference signal, $r(n)$ is the filtered-x signal, $y(n)$ is the control signal fed to the control source, and $e(n)$ denotes the error signal. $G_1(z)$ and $G_2(z)$ represent the primary paths from the noise source to microphones M1 and M2, while $H_1(z)$ and $H_2(z)$ denote the secondary paths from the secondary source to microphones M1 and M2, respectively. The sound absorption performance depends on the amplitude of the reflected wave $P_r(\omega)$ and is independent of its phase. Given the amplitude for the coefficient of $P_r(\omega)$ on the left side of the Eq. (6) is a constant, the error signal can be defined accordingly as

$$E(\omega) = P_1(\omega)e^{-j\omega\tau} - P_2(\omega). \tag{7}$$

The corresponding z-domain error signal $E(z)$ of Eq. (7) can be expressed as

$$E(z) = P_1(z)z^{-N} - P_2(z), \tag{8}$$

where $N = \tau \cdot f_s$ and f_s represents the sampling rate of the system. Meanwhile, $P_1(z)$ and $P_2(z)$ can also be represented by the primary sound pressure and the secondary sound pressure, i.e.,

$$P_1(z) = P_{1p}(z) + P_{1s}(z), \tag{9}$$

$$P_2(z) = P_{2p}(z) + P_{2s}(z), \tag{10}$$

where $P_{1p}(z) = X(z)G_1(z)$ and $P_{1s}(z) = Y(z)H_1(z)$ represent the primary and secondary acoustic signals at microphone

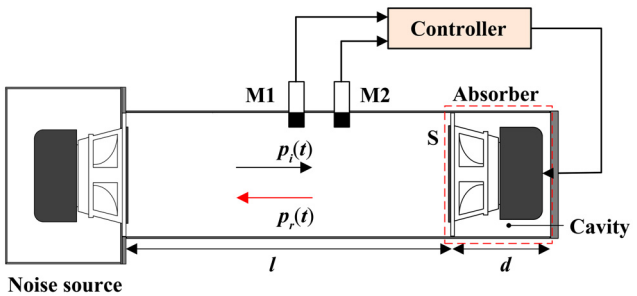

FIG. 1. (Color online) The schematic diagram of the designed active absorber. The main structure of the absorber with thickness d is marked by the red dashed box, which contains the loudspeaker and the cavity.

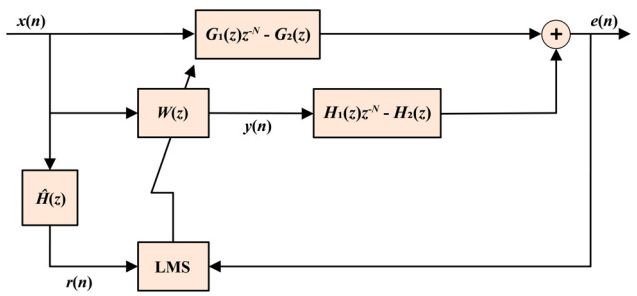

FIG. 2. (Color online) Module diagram illustrating the FxLMS algorithm for current active absorbers.

https://doi.org/10.1121/10.0028196

M1, respectively, while $P_{2p}(z) = X(z)G_2(z)$ and $P_{2s}(z) = Y(z)H_2(z)$ denote the primary and secondary acoustic signals at microphone M2, respectively. $X(z)$ and $Y(z)$ are the z-transform of the reference signal $x(n)$ and the secondary source signal $y(n)$, respectively. Bringing Eqs. (9) and (10) into Eq. (8) yields

$$E(z) = X(z)\left[G_1(z)z^{-N} - G_2(z)\right] + Y(z)\left[H_1(z)z^{-N} - H_2(z)\right]. \quad (11)$$

At this point, microphones M1 and M2 can be considered as a virtual microphone, termed M. The primary path of the virtual microphone M is $G(z) = G_1(z)z^{-N} - G_2(z)$, while the secondary path is $H(z) = H_1(z)z^{-N} - H_2(z)$, as shown in Fig. 2. The corresponding time-domain error signal $e(n)$ of Eq. (8) can be calculated by the inverse z-transform as

$$e(n) = p_1(n-N) - p_2(n). \quad (12)$$

To minimize the energy of the error signal $e(n)$, the cost function $J(n)$ is defined as

$$J(n) = E\left[e^2(n)\right], \quad (13)$$

where $E(\cdot)$ is the expectation operator. Following the FxLMS algorithm, the update formula for the control filter coefficients $\mathbf{w}(n)$ can be derived as[50]

$$\mathbf{w}(n+1) = \mathbf{w}(n) - 2\mu e(n)\mathbf{r}(n), \quad (14)$$

where μ represents the convergence coefficient, $\mathbf{r}(n)$ is the filtered-x signal vector, which is obtained by filtering the reference signal $\mathbf{x}(n)$ by the secondary path model $\hat{\mathbf{h}}(n)$. $\hat{\mathbf{h}}(n) = \hat{\mathbf{h}}_1(n-N) - \hat{\mathbf{h}}_2(n)$ is the impulse response of the secondary path estimation $\hat{H}(z)$ in Fig. 2, with $\hat{\mathbf{h}}_1(n)$ and $\hat{\mathbf{h}}_2(n)$ being estimates of the true secondary paths $\mathbf{h}_1(n)$ and $\mathbf{h}_2(n)$, respectively.

B. Proposed adjustable active absorber

To expand the tunability of the absorber, this paper introduces a scheme that can not only realize broadband absorption with arbitrarily adjustable absorption coefficients, but also tunable absorption spectra where reflection is still enabled within certain frequency bands. Since the reflection coefficient is expressed as $R = P_r/P_i$, combining Eqs. (5) and (6) yields

$$R(\omega) = e^{-j\omega\tau} \cdot \frac{P_1(\omega)e^{-j\omega\tau} - P_2(\omega)}{P_2(\omega)e^{-j\omega\tau} - P_1(\omega)}. \quad (15)$$

Likewise, only controlling the amplitude of the reflection coefficient is enough to achieve a specific sound absorption coefficient. According to Eq. (15), the error signal $E(\omega)$ can be defined as

$$E(\omega) = P_1(\omega)e^{-j\omega\tau} - P_2(\omega) - R_0(P_2(\omega)e^{-j\omega\tau} - P_1(\omega)), \quad (16)$$

where R_0 is the target reflection coefficient, which corresponds to the desired target absorption coefficient $A_0 = 1 - |R_0|^2$. The corresponding z-domain error signal $E(z)$ of Eq. (16) can also be formulated as

$$E(z) = P_1(z)z^{-N} - P_2(z) - R_0(P_2(z)z^{-N} - P_1(z)). \quad (17)$$

Bringing Eqs. (9) and (10) into Eq. (17) yields

$$E(z) = X(z)\left[G_1(z)z^{-N} - G_2(z) - R_0(G_2(z)z^{-N} - G_1(z))\right] + Y(z)\left[H_1(z)z^{-N} - H_2(z) - R_0(H_2(z)z^{-N} - H_1(z))\right]. \quad (18)$$

Therefore, the primary path of the virtual microphone M is converted as $G(z) = G_1(z)z^{-N} - G_2(z) - R_0(G_2(z)z^{-N} - G_1(z))$, while the secondary path is converted as $H(z) = H_1(z)z^{-N} - H_2(z) - R_0(H_2(z)z^{-N} - H_1(z))$. The corresponding time-domain error signal $e(n)$ of Eq. (17) can also be calculated by the inverse z-transform as

$$e(n) = p_1(n-N) - p_2(n) - R_0(p_2(n-N) - p_1(n)). \quad (19)$$

The target absorption coefficient A_0 is obtained by minimizing the energy of $e(n)$ in Eq. (19). In contrast to Eq. (12), which requires only the reflected wave to achieve perfect broadband absorption, the proposed approach leverages both incident and reflected wave information to attain broadband absorption with adjustable absorption coefficients.

The control algorithm can be implemented using the FeLMS algorithm,[48] illustrated in Fig. 3. Compared to Fig. 2, the primary and secondary path models contain information about incident and reflected sound, allowing the algorithm to achieve broadband sound absorption with adjustable coefficients by setting different target reflection coefficients R_0. Additionally, a shaping filter $\mathbf{f}(n)$ is applied based on the FeLMS algorithm to filter the error signal and reference signal before updating the control filter $\mathbf{w}(n)$. This constrains the frequency band of the control filter and achieves spectrally tunable broadband sound absorption. In Fig. 3, $F(z)$ within the light blue box signifies the z-transform of the shaping filter $\mathbf{f}(n)$. The filtered error signal $e'(n)$ is obtained by filtering the error signal $e(n)$ by the shaping

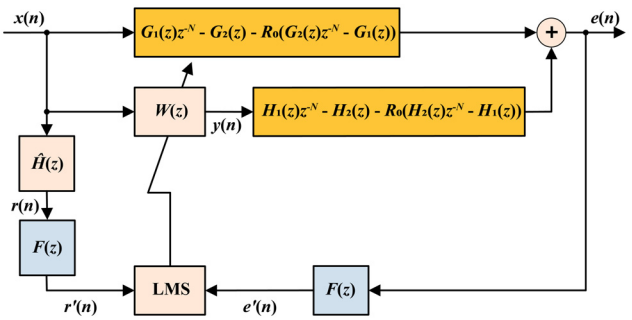

FIG. 3. (Color online) Module diagram illustrating the control algorithm for the designed active absorber.

filter $F(z)$, i.e., $e'(n) = e(n) * f(n)$, and the cost function is correspondingly modified to $J'(n)$ as

$$J'(n) = E\left[e'^2(n)\right]. \tag{20}$$

Like the derivation of the FxLMS algorithm, the update formula for the controller $\mathbf{w}(n)$ in the FeLMS algorithm can be derived as

$$\mathbf{w}(n+1) = \mathbf{w}(n) - 2\mu e'(n)\mathbf{r}'(n), \tag{21}$$

where $\mathbf{r}'(n)$ is the signal vector obtained by filtering $\mathbf{r}(n)$ by the shaping filter $F(z)$, i.e., $r'(n) = r(n) * f(n)$. At this point, the secondary path estimate $\hat{\mathbf{h}}(n)$ that generates the filtered reference signal vector $\mathbf{r}(n)$ is expressed as $\hat{\mathbf{h}}(n) = \hat{\mathbf{h}}_1(n-N) - \hat{\mathbf{h}}_2(n) - R_0(\hat{\mathbf{h}}_2(n-N) - \hat{\mathbf{h}}_1(n))$.

In the case where $F(z) = 1$, the FeLMS algorithm reverts to the FxLMS algorithm. In this scenario, the active absorber modulates solely the absorption coefficients according to the specified target reflection coefficient R_0. The update formula for the control filter $\mathbf{w}(n)$ in Eq. (21) is formally simplified as in Eq. (14); however, $e(n)$ and $\mathbf{r}(n)$ are different between the two. The two formulas are identical only when $R_0 = 0$.

III. EXPERIMENTS

To validate the effectiveness of the proposed active absorber, experiments were conducted in a circular standing wave tube shown in Fig. 4 with a diameter of $d_0 = 12$ cm, which has a cutoff frequency of 1658 Hz for the plane wave mode. The tube wall is made of 20 mm thick plexiglass, which provides good sound insulation, predicted by the mass law to exceed 25 dB above 150 Hz. The primary noise source, powered by an amplifier, was positioned at the left end of the tube, while the active absorber was placed at the opposite end, maintaining a spacing of $l = 1.5$ m. Acoustic foams were placed in front of the noise source to mitigate the influence of multiple sound wave reflections within the tube. The active absorber consists of a 4 in. Hivi B4N loudspeaker (Hivi, Guangzhou, China) (see detailed Thiele & Small parameters in Supplementary Table SI) and a cavity behind it with a thickness of $d = 82.5$ mm, surrounded by a 20 mm–thick plexiglass plate that can be considered as a hard boundary. To simplify the design of the experimental system, microphones M1 and M2, with a spacing of $s = 8$ cm, were employed as error microphones for the active absorber as well as measurement microphones. The absorption coefficients of active absorbers could be measured based on the transfer function method. The resulting measured sound absorption coefficient is denoted as A_{mea}, i.e.,

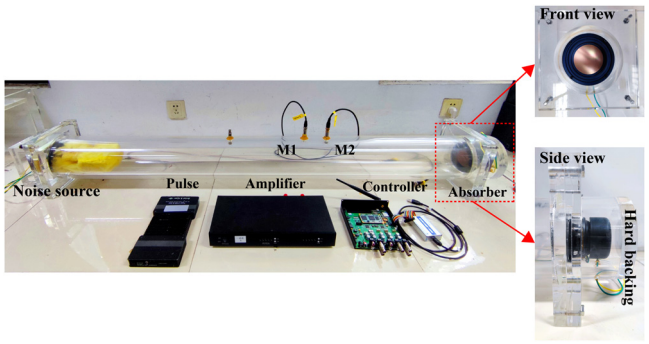

FIG. 4. (Color online) Photograph of the experimental setup based on a one-dimensional standing wave tube. The two subfigures depict the front and side views of the active absorber.

$$A_{\text{mea}} = 1 - |R_{\text{mea}}|^2, \tag{22}$$

$$R_{\text{mea}} = \frac{H_{12} - H_{\text{I}}}{H_{\text{R}} - H_{12}} e^{j2kx_1}, \tag{23}$$

where $H_{12} = p_2/p_1$ is the transfer function between the sound pressure signals measured by microphones M2 and M1, and $H_{\text{I}} = e^{-jks}$, $H_{\text{R}} = e^{jks}$. $k = \omega/c_0$ denotes the wave number in air, and x_1 refers to the distance from microphone M1 to the interface $\boldsymbol{S}$ of the active absorber.

During the experiments, to exclusively excite the plane wave mode, a low-pass white noise signal below 1600 Hz is generated by the B&K Pulse (Brüel & Kjær, Naerum, Denmark), which is then amplified to drive the noise source. Simultaneously, the signal is also fed into the controller to serve as the reference signal. The controller is implemented by employing a TMS320C6748 chip (Texas Instruments, Dallas, TX) with a sampling rate of $f_s = 16\,000$ Hz and a 1024-tapped finite impulse response (FIR) filter is embedded. The identification of secondary paths $\mathbf{h}_1(n)$ and $\mathbf{h}_2(n)$ is conducted using the least mean square (LMS) algorithm, employing two 512-tapped FIR filters with a modelling accuracy of up to 25 dB.

A. Realization of arbitrarily adjustable sound absorption coefficients

The shaping filter $F(z) = 1$ in Fig. 3 is set to explore the broadband sound absorption performance and adjustability of the absorption coefficient of the designed active absorber. Initially, the active sound absorption effect under the perfect absorption ($R_0 = 0$) condition is compared with the passive sound absorption effect, with results depicted in Fig. 5(a). Passive absorption denotes performance achieved by deactivating the active control and relying solely on the sound absorption capacity of the secondary source loudspeaker. It can be seen that in the 150–1600 Hz frequency band, the average sound absorption coefficient is merely 0.09, indicating poor performance in this scenario. By turning on the active control function and setting $R_0 = 0$ in the error signal, the active absorber can realize near-perfect broadband absorption performance in the frequency band of 150–1600 Hz with an average absorption coefficient of 0.98 when the controller converges. Figure 5(b) compares the reflected wave amplitudes for passive and active absorption to further demonstrate the attenuation of reflected wave energy by the active absorber. The results demonstrate that the designed active absorber significantly reduces the reflected wave energy and achieves near-perfect sound

https://doi.org/10.1121/10.0028196

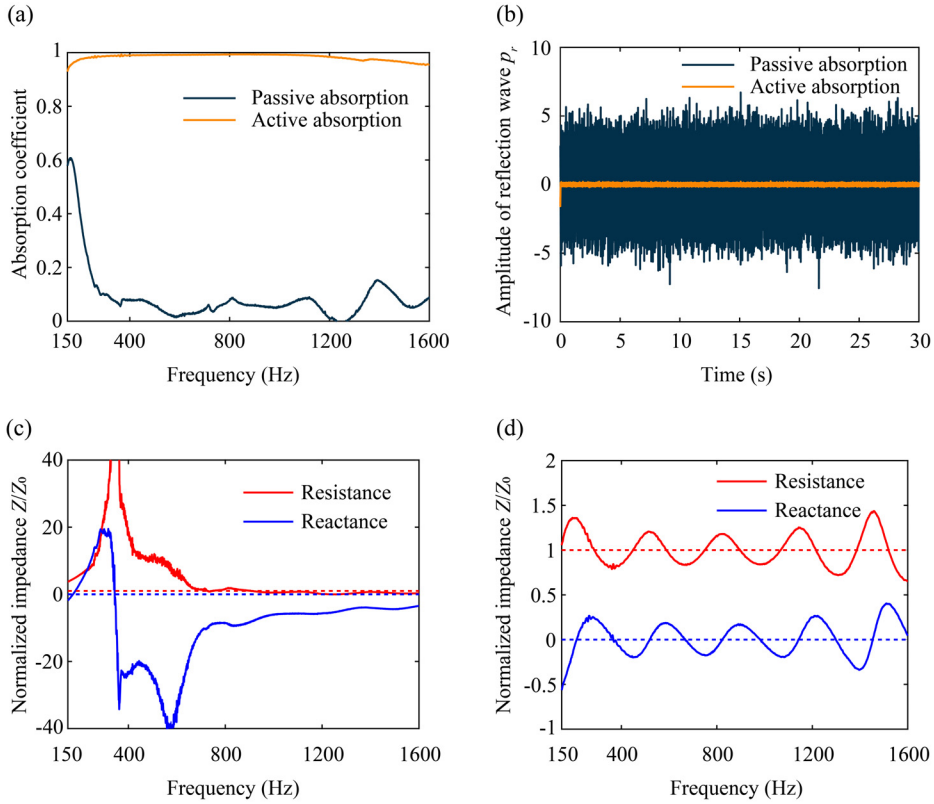

FIG. 5. (Color online) Comparison of the active absorption performance under the perfect absorption condition ($R_0 = 0$) with passive absorption solely by the secondary source loudspeaker. (a) Spectra of absorption coefficients for passive and active absorption, (b) the remaining amplitude of reflected waves after passive and active absorption, (c) and (d) normalized acoustic impedance at the absorber interface $\boldsymbol{S}$ for passive and active absorption. This acoustic impedance can be derived from the measured reflection coefficient R_{mea}, i.e., $Z/Z_0 = (1 + R_{\mathrm{mea}})/(1 - R_{\mathrm{mea}})$, where $Z_0 = \rho_0 c_0$ is the characteristic acoustic impedance of air. The red dashed line indicates the real part of Z_0, while the blue dashed line indicates the imaginary part of Z_0, providing a reference for evaluating the matching degree between the acoustic impedance at the absorber interface $\boldsymbol{S}$ and that of air.

absorption. This is attributed to the controller adjusting the acoustic impedance at the secondary source interface $\boldsymbol{S}$ to match the characteristic acoustic impedance Z_0 of the air [refer to Figs. 5(c) and 5(d)], thereby significantly enhancing the absorption performance of the absorber.

The designed active absorber also enables broadband absorption with arbitrarily adjustable absorption coefficient by setting different target reflection coefficients R_0 in the error signal when the shaping filter $F(z) = 1$. Five cases of $R_0 = 0$, 0.3, 0.5, 0.7, and 0.9 are demonstrated and the results are shown in Fig. 6(a). When the controller converges, the active absorber exhibits flat broadband absorption spectra with adjustable absorption coefficients within the 150–1600 Hz frequency band, showing an effective control bandwidth exceeding three octaves. The residual amplitude of the reflected wave is compared across different R_0 values in Fig. 6(b), as expected decreasing R_0 results in a reduction of the residual reflected wave amplitude. The average absorption coefficients of the measured absorption spectra within the 150–1600 Hz band for these five cases are 0.98, 0.94, 0.82, 0.62, and 0.33, respectively, aligning well with the theoretical absorption coefficient $A_0 = 1 - |R_0|^2$, as shown in Fig. 6(c). The slight deviation can be attributed to the fact that the acoustic time delay τ between microphones M1 and M2 results in a non-integer sampling point $N = \tau \cdot f_s$, which had to be rounded off due to the utilization of a digital signal processor (DSP) in the experiments. Although only five cases are illustrated here, it is reasonable to infer that the designed active absorber can achieve arbitrary absorption coefficients ranging from 0 to 1, showcasing its versatile broadband tunability. This capability holds significant potential for optimizing acoustic characteristics in multipurpose rooms where different absorption coefficients and reverberation times are needed.

Subsequently, the effect of the active absorber on the sound field distribution in the tube is analyzed in detail. Utilizing the finite element model developed with commercial software COMSOL Multiphysics 5.6 (COMSOL, Stockholm, Sweden; see detailed model in Supplementary Note S1), and imposing the experimentally measured interfacial impedance of the active absorber at the right end of the waveguide, the sound pressure level (SPL) distribution in the tube for various target reflection coefficients R_0 of the active absorber can be obtained, as shown in Fig. 7. Figure 7(a) illustrates the SPL distribution in the tube with a hard boundary imposed at the waveguide's right end. Obvious standing wave patterns can be observed, indicating a highly inhomogeneous sound field. Figure 7(b) shows the SPL distribution when the active absorber is off, relying only on the loudspeaker's passive absorption capability. According to Fig. 5(a), since the loudspeaker has limited absorbing ability at 165 Hz and almost none at other frequencies, the sound field distribution in the tube is still a standing wave field with large fluctuation. When the active absorber is turned on and the target reflection coefficient $R_0 = 0.5$ is set, the SPL distribution is illustrated in Fig. 7(c). The result demonstrates significantly reduced fluctuation within all the 150–1600 Hz bands. Setting the target reflection coefficient $R_0 = 0$ further homogenizes the sound field, as shown in Fig. 7(d). These results further confirm the desired

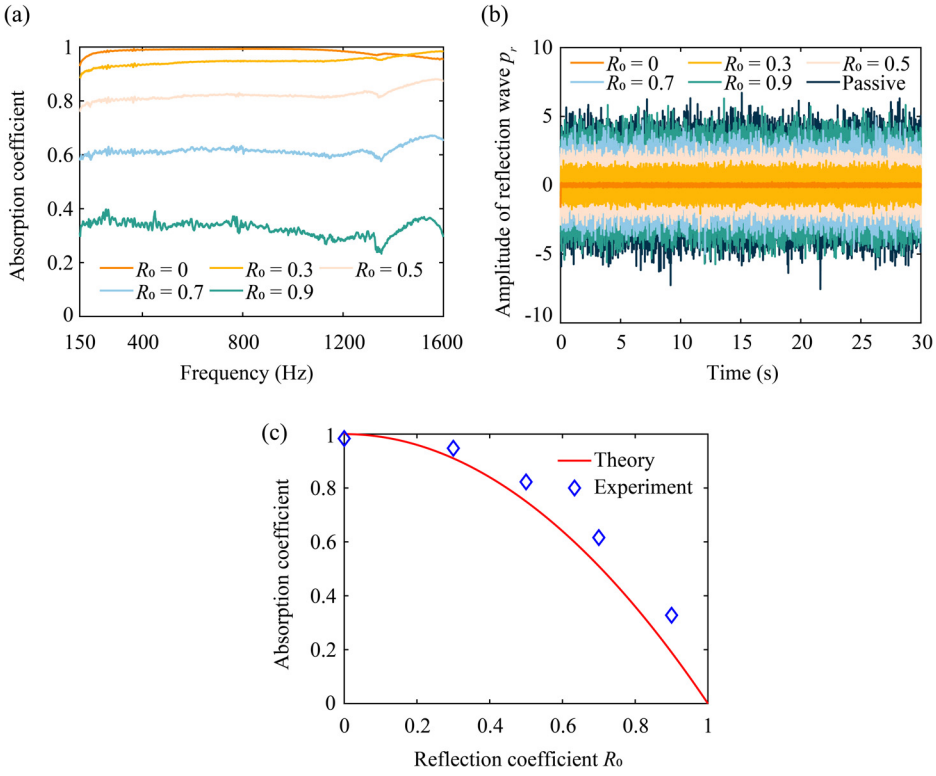

FIG. 6. (Color online) Setting various values of the target reflection coefficient R_0 in the error signal to achieve different sound absorption performance. (a) Acoustic absorption spectra for different R_0 values, (b) comparison of the remaining amplitude of the reflected wave after active and passive absorption, (c) comparison of measured average absorption coefficients with theoretical values.

absorption performance and indicate the great potential of the designed active absorber for modulating sound field characteristics in confined spaces.

B. Realization of spectrally tunable broadband sound absorption

By employing a shaping filter $\mathbf{f}(n)$, the active absorber can achieve broadband sound absorption with spectrally tunable characteristics. The time-domain impulse response and amplitude-frequency response of a 512-tapped band-stop shaping filter $\mathbf{f}(n)$ are depicted in Figs. 8(a) and 8(b), respectively. $\mathbf{f}(n)$ has a stop band frequency range of 700–1000 Hz, and its use to filter the error signal means that there is no need to eliminate the reflected wave within 700–1000 Hz. This characteristic is particularly useful in cases where higher reflection in a particular band is desired.

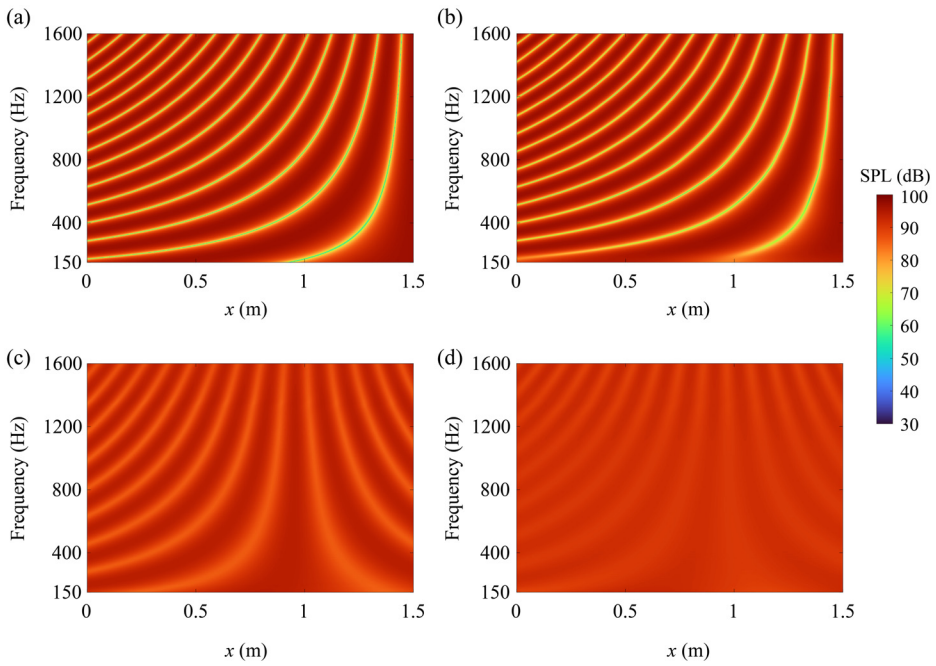

FIG. 7. (Color online) The SPL distribution in the waveguide when the active absorber has different target reflection coefficients R_0. (a) The hard boundary is imposed at the right end of the waveguide for comparison, (b) passive absorption with the active absorber turned off, (c) active absorption with $R_0 = 0.5$, corresponding to partial absorption, (d) active absorption with $R_0 = 0$, corresponding to perfect absorption.

https://doi.org/10.1121/10.0028196

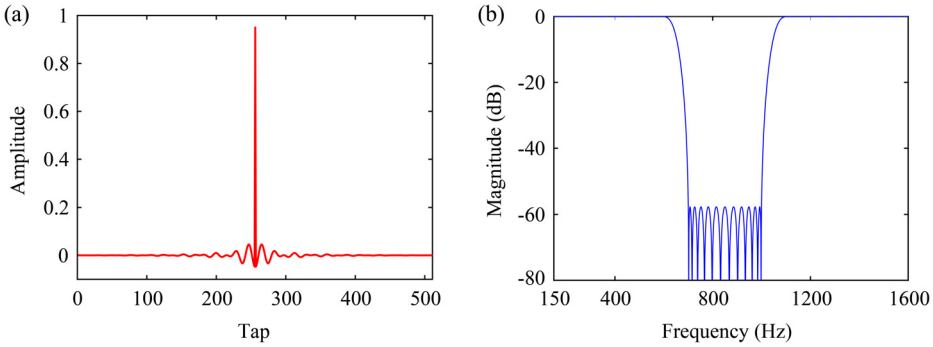

FIG. 8. (Color online) Designed band-stop shaping filter $\mathbf{f}(n)$. (a) Time-domain impulse response of $\mathbf{f}(n)$, (b) amplitude-frequency response of $\mathbf{f}(n)$.

By setting the target reflection coefficient $R_0 = 0$ in Eq. (21) and filtering the error signal with the shaping filter $\mathbf{f}(n)$, the measured sound absorption spectrum is shown in Fig. 9(a). Comparing the active absorption effect before and after applying the shaping filter, a noticeable reduction of absorption performance within the stop band range of the filter can be observed. This reduction indicates the enhanced reflection of sound waves within this frequency range, consistent with the anticipated outcome. With the shaping filter $\mathbf{f}(n)$ utilized, the active absorber exhibits an average absorption coefficient of merely 0.15 within the 700–1000 Hz band, while other bands remain almost unaffected, achieving an average absorption coefficient of up to 0.97. The spectrally tunable capacity stems from that the response of the control filter $\mathbf{w}(n)$ within the stop band range is constrained, as illustrated in Fig. 9(b). Within the partial stop band range, the absorption coefficient may exhibit slight negativity, attributed to the controller's response not fully constrained to zero. This amplifies the reflection wave within the stop band compared to the fully passive case, in line with our design objective. The excessive reflection wave, on the other hand, can be alleviated by incorporating a fine-tuned shaping filter design or passive absorption materials if it is not desired.

Assigning different values to the target reflection coefficient R_0 in Eq. (21), the proposed active absorber achieves not only a tunable sound absorption spectrum but also modulation of the absorption coefficient in the passband. Figure 10 compares the sound absorption effects for $R_0 = 0$ and $R_0 = 0.5$. When $R_0 = 0.5$, the absorption coefficient within the passband decreases accordingly, with an average absorption coefficient of 0.81, closely aligning with the theoretical value of $A_0 = 1 - |R_0|^2 = 0.75$. Therefore, the system demonstrates the ability to achieve broadband sound absorption performance with a flexibly tunable spectrum. Furthermore, a variety of absorption spectra can be synthesized by simply changing the shaping filter $\mathbf{f}(n)$. Such an approach offers tremendous flexibility in reverse engineering by first defining the desired absorption spectrum and then adjusting the target reflection coefficient R_0 and shaping filter $\mathbf{f}(n)$ to match this spectrum.

IV. CONCLUSIONS

This study presents an active absorber with flexible tunability in a one-dimensional standing wave tube. The two-microphone method is employed to separate the incident and reflected waves so that the error signal can be synthesized, enabling broadband adjustment of the acoustic absorption performance. This active absorber demonstrates remarkable near-perfect absorption within the 150–1600 Hz frequency band, with an average absorption coefficient of 0.98. Through manipulation of the target reflection coefficient in the error signal, the absorber achieves a tunable absorption coefficient spanning from 0 to 1 across more than three octave bands. Experimental results closely align with theoretical predictions. Utilizing the FeLMS algorithm with a band-stop filter, this active absorber obtains spectrally tunable broadband sound absorption, selectively reflecting specific frequency bands while absorbing the rest. By adjusting the target reflection coefficient in the error signal, the absorption coefficient in the passband is also customizable. Importantly, these modulation capabilities are realized

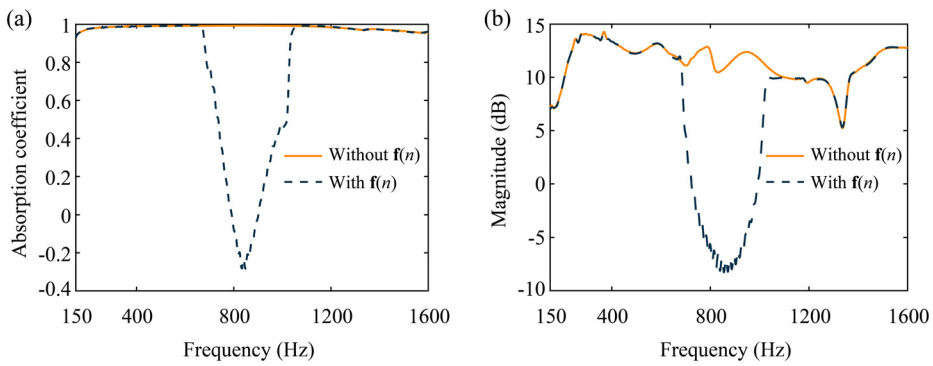

FIG. 9. (Color online) Comparison of sound absorption obtained with and without the shaping filter $\mathbf{f}(n)$. (a) Spectra of absorption coefficient, (b) amplitude-frequency response of the control filter.

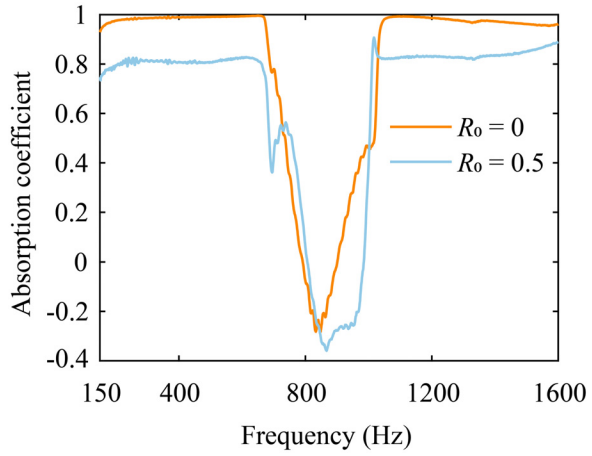

FIG. 10. (Color online) Comparison of the sound absorption effect achieved by setting the target reflection coefficient R_0 to 0 and 0.5 in the error signal when utilizing the shaping filter $\mathbf{f}(n)$.

solely through programming in the digital controller, without any alterations to the physical structure of the active absorber. Although the active absorber has only been demonstrated in a one-dimensional waveguide, the concept applies to higher dimensions in which a large-area active absorber array can be expected by combining more units.[46] The obtained findings highlight the flexible nature of the designed active absorber, promising versatile solutions for controlling acoustic environments in confined spaces and offering insights for potential applications in other scenarios.

SUPPLEMENTARY MATERIAL

See the supplementary material for referenced additional table and note mentioned in the main manuscript text.

ACKNOWLEDGMENTS

This work was supported by the National Natural Science Foundation of China (Grant No. 12274221).

AUTHOR DECLARATIONS

Conflict of Interest

The authors have no conflicts to disclose.

DATA AVAILABILITY

The data that support the findings of this study are available from the corresponding author upon reasonable request.

[1]M. Cairoli, "Architectural customized design for variable acoustics in a multipurpose auditorium," Appl. Acoust. **140**, 167–177 (2018).
[2]H. Kuttruff, *Room Acoustics* (CRC Press, Boca Raton, FL, 2016).
[3]A. Merkel, G. Theocharis, O. Richoux, V. Romero-García, and V. Pagneux, "Control of acoustic absorption in one-dimensional scattering by resonant scatterers," Appl. Phys. Lett. **107**, 244102 (2015).
[4]Z. X. Xu, H. Y. Meng, A. Chen, J. Yang, B. Liang, and J. C. Cheng, "Tunable low-frequency and broadband acoustic metamaterial absorber," J. Appl. Phys. **129**, 094502 (2021).
[5]J. F. Li, W. Q. Wang, Y. B. Xie, B. I. Popa, and S. A. Cummer, "A sound absorbing metasurface with coupled resonators," Appl. Phys. Lett. **109**, 091908 (2016).
[6]S. Huang, X. Fang, X. Wang, B. Assouar, Q. Cheng, and Y. Li, "Acoustic perfect absorbers via Helmholtz resonators with embedded apertures," J. Acoust. Soc. Am. **145**, 254–262 (2019).
[7]H. Ding, N. Wang, S. Qiu, S. Huang, Z. Zhou, C. Zhou, B. Jia, and Y. Li, "Broadband acoustic meta-liner with metal foam approaching causality-governed minimal thickness," Int. J. Mech. Sci. **232**, 107601 (2022).
[8]H. Ryoo and W. Jeon, "Broadband sound absorption using multiple hybrid resonances of acoustic metasurfaces," Int. J. Mech. Sci. **229**, 107508 (2022).
[9]Z. Zhou, S. Huang, D. Li, J. Zhu, and Y. Li, "Broadband impedance modulation via non-local acoustic metamaterials," Natl. Sci. Rev. **9**, nwab171 (2022).
[10]Z. Mei, X. Li, Y. Lyu, J. Sang, X. Cheng, and J. Yang, "Broadband sound absorption based on impedance decoupling and modulation mechanisms," J. Acoust. Soc. Am. **154**, 3479–3486 (2023).
[11]C. Shao, Y. Z. Zhu, H. Y. Long, C. Liu, Y. Cheng, and X. J. Liu, "Metasurface absorber for ultra-broadband sound via over-damped modes coupling," Appl. Phys. Lett. **120**, 083504 (2022).
[12]H. Y. Long, Y. Cheng, J. C. Tao, and X. J. Liu, "Perfect absorption of low-frequency sound waves by critically coupled subwavelength resonant system," Appl. Phys. Lett. **110**, 023502 (2017).
[13]C. R. Chen, Z. B. Du, G. K. Hu, and J. Yang, "A low-frequency sound absorbing material with subwavelength thickness," Appl. Phys. Lett. **110**, 221903 (2017).
[14]Y. Li and B. M. Assouar, "Acoustic metasurface-based perfect absorber with deep subwavelength thickness," Appl. Phys. Lett. **108**, 063502 (2016).
[15]C. Zhang and X. H. Hu, "Three-dimensional single-port labyrinthine acoustic metamaterial: Perfect absorption with large bandwidth and tunability," Phys. Rev. Appl. **6**, 064025 (2016).
[16]M. Yang, S. Y. Chen, C. Fu, and P. Sheng, "Optimal sound-absorbing structures," Mater. Horiz. **4**, 673–680 (2017).
[17]H. Y. Long, C. Shao, C. Liu, Y. Cheng, and X. J. Liu, "Broadband near-perfect absorption of low-frequency sound by subwavelength metasurface," Appl. Phys. Lett. **115**, 103503 (2019).
[18]H. Long, C. Liu, C. Shao, Y. Cheng, K. Chen, X. Qiu, and X. Liu, "Subwavelength broadband sound absorber based on a composite metasurface," Sci. Rep. **10**, 13823 (2020).
[19]C. Liu, Z. Yang, X. Liu, J. H. Wu, and F. Ma, "Ultra-broadband acoustic absorption with inhomogeneous high-order Fabry–Pérot resonances," APL Mater. **11**, 101122 (2023).
[20]K. Donda, Y. F. Zhu, S. W. Fan, L. Y. Cao, Y. Li, and B. Assouar, "Extreme low-frequency ultrathin acoustic absorbing metasurface," Appl. Phys. Lett. **115**, 173506 (2019).
[21]J. Mei, G. Ma, M. Yang, Z. Yang, W. Wen, and P. Sheng, "Dark acoustic metamaterials as super absorbers for low-frequency sound," Nat. Commun. **3**, 756 (2012).
[22]G. Ma, M. Yang, S. Xiao, Z. Yang, and P. Sheng, "Acoustic metasurface with hybrid resonances," Nat. Mater. **13**, 873–878 (2014).
[23]M. Yang, C. Meng, C. X. Fu, Y. Li, Z. Y. Yang, and P. Sheng, "Subwavelength total acoustic absorption with degenerate resonators," Appl. Phys. Lett. **107**, 104104 (2015).
[24]Z. Lu, M. Shrestha, and G.-K. Lau, "Electrically tunable and broader-band sound absorption by using micro-perforated dielectric elastomer actuator," Appl. Phys. Lett. **110**, 182901 (2017).
[25]Y. Aurégan, "Ultra-thin low frequency perfect sound absorber with high ratio of active area," Appl. Phys. Lett. **113**, 201904 (2018).
[26]W. Ao, J. Ding, L. Fan, and S.-y. Zhang, "A robust actively-tunable perfect sound absorber," Appl. Phys. Lett. **115**, 193506 (2019).
[27]S. C. Qu, M. Yang, Y. F. Xu, S. W. Xiao, and N. X. Fang, "Reverberation time control by acoustic metamaterials in a small room," Build. Environ. **244**, 110753 (2023).
[28]Y. F. Zhu, S. W. Fan, L. Y. Cao, K. Donda, and B. Assouar, "Acoustic meta-equalizer," Phys. Rev. Appl. **14**, 014038 (2020).
[29]C. Olivier, A. Maddi, G. Poignand, and G. Penelet, "Asymmetric transmission and coherent perfect absorption in a periodic array of thermoacoustic cells," J. Appl. Phys. **131**, 244701 (2022).
[30]A. Maddi, C. Olivier, G. Poignand, G. Penelet, V. Pagneux, and Y. Aurégan, "Frozen sound: An ultra-low frequency and ultra-broadband non-reciprocal acoustic absorber," Nat. Commun. **14**, 4028 (2023).

https://doi.org/10.1121/10.0028196

[31]H. K. Zhang, Q. Y. Wang, M. Fink, and G. C. Ma, "Optimizing multi-user indoor sound communications with acoustic reconfigurable metasurfaces," Nat. Commun. **15**, 1270 (2024).
[32]T. T. Koutserimpas, E. Rivet, H. Lissek, and R. Fleury, "Active acoustic resonators with reconfigurable resonance frequency, absorption, and bandwidth," Phys. Rev. Appl. **12**, 054064 (2019).
[33]C. Cong, J. Tao, and X. Qiu, "A multi-tone sound absorber based on an array of shunted loudspeakers," Appl. Sci. **8**, 2484 (2018).
[34]P. Zhang, C. Cong, J. Tao, and X. Qiu, "Dual frequency sound absorption with an array of shunt loudspeakers," Sci. Rep. **10**, 10806–8 (2020).
[35]Y. Zhang, Y.-J. Chan, and L. Huang, "Thin broadband noise absorption through acoustic reactance control by electro-mechanical coupling without sensor," J. Acoust. Soc. Am. **135**, 2738–2745 (2014).
[36]Y. Zhang, C. Wang, and L. Huang, "Tuning of the acoustic impedance of a shunted electro-mechanical diaphragm for a broadband sound absorber," Mech. Syst. Sig. Process. **126**, 536–552 (2019).
[37]J. Tao, R. Jing, and X. Qiu, "Sound absorption of a finite microperforated panel backed by a shunted loudspeaker," J. Acoust. Soc. Am. **135**, 231–238 (2014).
[38]X. Li, Z. Cao, Z. Li, and B. Liu, "Sound absorption of a shunt loudspeaker on a perforated plate," Appl. Acoust. **193**, 108776 (2022).
[39]Z. Cao, X. Li, and B. Liu, "Broadband sound absorption of a hybrid absorber with shunt loudspeaker and perforated plates," Appl. Acoust. **203**, 109185 (2023).
[40]R. Boulandet and H. Lissek, "Toward broadband electroacoustic resonators through optimized feedback control strategies," J. Sound Vibr. **333**, 4810–4825 (2014).
[41]E. Rivet, S. Karkar, and H. Lissek, "Broadband low-frequency electroacoustic absorbers through hybrid sensor-/shunt-based impedance control," IEEE Trans. Control Syst. Technol. **25**, 63–72 (2017).
[42]S. Sergeev, R. Fleury, and H. Lissek, "Ultrabroadband sound control with deep-subwavelength plasmacoustic metalayers," Nat. Commun. **14**, 2874 (2023).
[43]M. Volery, X. X. Guo, and H. Lissek, "Robust direct acoustic impedance control using two microphones for mixed feedforward-feedback controller," Acta Acust. **7**, 2 (2023).
[44]S. Beyene and R. A. Burdisso, "A new hybrid passive–active noise absorption system," J. Acoust. Soc. Am. **101**, 1512–1515 (1997).
[45]P. Cobo, A. Fernández, and O. Doutres, "Low-frequency absorption using a two-layer system with active control of input impedance," J. Acoust. Soc. Am. **114**, 3211–3216 (2003).
[46]P. Cobo and M. Cuesta, "Measuring hybrid passive-active sound absorption of a microperforated liner at oblique incidence," J. Acoust. Soc. Am. **125**, 185–190 (2009).
[47]F. An, P. Zhao, X. Li, Q. Wu, and B. Liu, "Active impedance control of a loudspeaker and its parallel combination with porous materials for broadband sound absorption," Mech. Syst. Signal Process. **206**, 110909 (2024).
[48]S. M. Kuo and J. M. Tsai, "Residual noise shaping technique for active noise-control systems," J. Acoust. Soc. Am. **95**, 1665–1668 (1994).
[49]X. Ma, D. Yurchenko, K. Chen, L. Wang, Y. Liu, and K. Yang, "Structural acoustic controlled active micro-perforated panel absorber for improving wide-band low frequency sound absorption," Mech. Syst. Signal Process. **178**, 109295 (2022).
[50]S. Elliott, *Signal Processing for Active Control* (Academic Press, London, 2001).
[51]A. V. Oppenheim and R. W. Schafer, *Discrete-Time Signal Processing* (Prentice Hall Press, Hoboken, NJ, 1999).